Journal of Ginseng Research 47 (2023) 97–105

Contents lists available at ScienceDirect

Journal of Ginseng Research

journal homepage: https://www.sciencedirect.com/journal/journal-of-ginseng-research

Research Article

A systematic exploration of ginsenoside Rg5 reveals anti-inflammatory functions in airway mucosa cells

Hyojin Heo [a, 1], Yumin Kim [b, c, 1], Byungsun Cha [d, 1], Sofia Brito [a, 1], Haneul Kim [d], Hyunjin Kim [d], Bassiratou M. Fatombi [d], So Young Jung [a], So Min Lee [d], Lei Lei [d], Sang Hun Lee [d], Geon-woo Park [a, b], Byeong-Mun Kwak [e, **], Bum-Ho Bin [a, d, ***], Ji-Hwan Park [b, ****], Mi-Gi Lee [f, *]

[a] Department of Applied Biotechnology, Ajou University, Suwon, Republic of Korea
[b] Korea Bioinformation Center, Korea Research Institute of Bioscience & Biotechnology, Daejeon, Republic of Korea
[c] Department of Biomedical Science and Engineering, Gwangju Institute of Science & Technology, Republic of Korea
[d] Department of Biological Sciences, Ajou University, Suwon, Republic of Korea
[e] Department of Meridian and Acupoint, College of Korean Medicine, Semyung University, Chungbuk, Republic of Korea
[f] Bio-Center, Gyeonggi-do Business and Science Accelerator, Suwon, Republic of Korea

ARTICLE INFO

Article history:
Received 18 May 2021
Received in revised form
20 June 2022
Accepted 20 June 2022
Available online 5 July 2022

Keywords:
Airway mucosa inflammation
Ginsenoside Rg5
Mucin overproduction
Lipid droplet
Reactive oxygen species

ABSTRACT

Background: Hyperactivated airway mucosa cells overproduce mucin and cause severe breathing complications. Here, we aimed to identify the effects of saponins derived from *Panax ginseng* on inflammation and mucin overproduction.

Methods: NCI–H292 cells were pre-incubated with 16 saponins derived from *P. ginseng*, and mucin overproduction was induced by treatment with phorbol 12-myristate 13-acetate (PMA). Mucin protein MUC5AC was quantified by enzyme-linked immunosorbent assay, and mRNA levels were analyzed using quantitative polymerase chain reaction (qPCR). Moreover, we performed a transcriptome analysis of PMA-treated NCI–H292 cells in the absence or presence of Rg5, and differential gene expression was confirmed using qPCR. Phosphorylation levels of signaling molecules, and the abundance of lipid droplets, were measured by western blotting, flow cytometry, and confocal microscopy.

Results: Ginsenoside Rg5 effectively reduced MUC5AC secretion and decreased *MUC5AC* mRNA levels. A systematic functional network analysis revealed that Rg5 upregulated cholesterol and glycerolipid metabolism, resulting in the production of lipid droplets to clear reactive oxygen species (ROS), and modulated the mitogen-activated protein kinase and nuclear factor (NF)-κB signaling pathways to regulate inflammatory responses. Rg5 induced the accumulation of lipid droplets and decreased cellular ROS levels, and N-acetyl-L-cysteine, a ROS inhibitor, reduced MUC5AC secretion via Rg5. Furthermore, Rg5 hampered the phosphorylation of extracellular signal-regulated kinase and p38 proteins, affecting the NF-κB signaling pathway and pro-inflammatory responses.

Conclusion: Rg5 alleviated inflammatory responses by reducing mucin secretion and promoting lipid droplet-mediated ROS clearance. Therefore, Rg5 may have potential as a therapeutic agent to alleviate respiratory disorders caused by hyperactivation of mucosa cells.

**** Corresponding author. Korea Bioinformation Center, Korea Research Institute of Bioscience & Biotechnology, Republic of Korea.
*** Corresponding author. Department of Biological Sciences, Ajou University, Suwon, 16499, Republic of Korea.
** Corresponding author. Department of Meridian and Acupoint, College of Korean Medicine, Semyung University, Chungbuk, 27136, Republic of Korea.
* Corresponding author. Bio-Center, Gyeonggi-do Business and Science Accelerator, Suwon, 16229, Republic of Korea.
E-mail addresses: bmkwak@semyung.ac.kr (B.-M. Kwak), bhb@ajou.ac.kr (B.-H. Bin), jhpark706@kribb.re.kr (J.-H. Park), migi1231@gmail.com (M.-G. Lee).
[1] These authors contributed equally to this manuscript.

https://doi.org/10.1016/j.jgr.2022.06.001

1. Introduction

Respiratory diseases are pathological conditions that affect proper lung function. Airway disorders, such as asthma, chronic obstructive pulmonary disease, bronchiectasis, and pulmonary cystic fibrosis, are characterized by severe inflammation and mucus overproduction [1,2]. Mucus is produced in the submucosal and mucosal cells of the airway epithelium. The primary function of mucus is debris removal, which is essential to prevent microbial invasion and aid in airway moisture loss [3]. Mucus contains several large glycoproteins (mucins [MUCs]), which provide viscoelasticity and play major roles as defense-related molecules in the lungs [4]. In human airway epithelial cells, over 20 MUC proteins are expressed. Among them, MUC5AC, a human mucin 5AC protein encoded by the *MUC5AC* gene, is primarily expressed in airway surface epithelial goblet cells, and its overexpression is associated with chronic inflammatory airway diseases [5,6].

Contemporary drugs for treating respiratory tract inflammation are disadvantageous in terms of high cost and adverse side effects. By contrast, natural products are readily accessible and can be used as a crucial reserve of novel therapies for respiratory diseases because of their renewable nature [7]. However, the efficacy and safety of many natural products remain unclear owing to our inadequate understanding of their complex molecular mechanisms. Therefore, it is necessary to further investigate novel natural anti-inflammatory drugs to address this issue [8,9].

Heat treatment is a method that can be applied to plant products to enhance their physiological activity. Heat treatment of ginseng is known to induce structural changes due to the conversion of ginsenosides, resulting in improved therapeutic efficacy [10,11]. In this process, ginsenosides (ginseng saponins), i.e., Ra1, Ra2, Ra3, Rf2, Rg4, Rg5, Rg6, Rk1, Rs1, and Rs2, are produced via the heat transformation and deglycosylation of naturally occurring ginsenosides [12]. In particular, large amounts of ginsenoside Rg5 can be produced during the steaming process, which was first studied to alleviate inflammatory lung disease [13]. Rg5 ($C_{42}H_{70}O_{12}$) is a principal component of red ginseng and belongs to a family of protopanaxadiol ginsenosides [14]. This compound has been shown to hinder cancer progression and has beneficial effects on the skin, neurons, and microglia [13,15,16]. However, no reports have demonstrated the molecular mechanisms through which Rg5 affects respiratory diseases.

Accordingly, in this study, we evaluated the molecular mechanisms of Rg5 in mucous production and inflammation using human lung mucosal epithelial cells.

2. Materials and methods

2.1. Cell culture and reagents

NCI–H292 human pulmonary mucoepidermoid carcinoma cells were purchased from American Type Culture Collection (Manassas, VA, USA). The cells were cultured at 37°C under a 5% CO_2 using high-glucose Dulbecco's modified Eagle medium (HyClone, Logan, UT, USA) supplemented with 10% fetal bovine serum and 1% penicillin-streptomycin (Welgene, Gyeongsan, Republic of Korea). Phorbol 12-myristate 13-acetate (PMA) and N-acetyl-L-cysteine (NAC) were purchased from Sigma-Aldrich (St. Louis, MO, USA). Rg5 was purchased from the Ambo Institute (Daejeon, Republic of Korea).

2.2. Quantitative real-time polymerase chain reaction (qPCR)

Total RNA from NCI–H292 cells pretreated with Rg5 (0, 10, 50, or 100 μg/mL for 2 h) and treated with PMA (10 mg/mL for 1 h) was extracted using TRIzol RNA Reagent (Life Technologies, Waltham, MA, USA), as recommended by the manufacturer. For qPCR, 2 μg RNA was subjected to reverse transcription at 37°C for 1 h using AccuPower RT PreMix (Bioneer, Daejeon, Korea). Human gene primers were purchased from Bionics (Seoul, Korea; Table S1), and mRNA levels were analyzed using QGreenBlue 2 × qPCR Master Mix (CellSafe, Yongin, Korea) on an AriaMX Real-TimePCR System (Agilent, Santa Clara, CA, USA). Gene expression was normalized to that of glyceraldehyde 3-phosphate dehydrogenase (*GAPDH*) using the comparative $2^{-\Delta\Delta Ct}$ method.

2.3. MUC secretion assay

The concentrations of MUC5AC in bile and serum were measured using a human MUC5AC enzyme-linked immunosorbent assay (ELISA) kit (cat. L190912437; USCN Life Science, Wuhan, China). The microtiter plate provided in this kit was precoated with biotin-conjugated anti-MUC5AC antibodies. Standards (0, 78, 156, 312, 625, 1250, 2500, or 5000 pg/mL standard diluent solution) and NCI–H292 cells pretreated with Rg5 (0, 10, 50, or 100 μg/mL for 30 min) and treated with PMA (10 mg/mL for 15 min) were then added to the appropriate microtiter plate wells. Next, avidin conjugated to horseradish peroxidase was added to each microplate well, and the plates were incubated at 37°C. After adding 3,3,5,5-tetramethylbenzidine substrate solution, the color change was measured at 450 nm using a microplate spectrophotometer (SpectraMax 190; Molecular Devices, San Jose, CA, USA). The MUC5AC concentration in each sample was determined by comparing its optical density with that of the standard curve.

2.4. Cell viability

Cell viability was assessed using 3-(4,5-dimethylthiazol-2-yl)-2,5-diphenyltetrazolium bromide (MTT) assays (Sigma-Aldrich). The cells were seeded in 96-well plates (1×10^4 cells/well), incubated overnight, and treated with varying concentrations of Rg5 for 24 h. MTT solution was added to the medium in each well at a concentration of 0.20 μg/μL, and plates were incubated for 4 h at 37°C. After confirming formazan formation, medium was discarded, and crystals were solubilized in 150 μL/well dimethyl sulfoxide (cat. D2650; Sigma-Aldrich). The absorption was measured at 570 nm on a microplate spectrophotometer.

2.5. RNA isolation and gene expression profiling

Total RNA was isolated from NCI–H292 cells treated with or without Rg5 using RNeasy Mini Kit columns (Qiagen, Hilden, Germany). RNA quality and quantity were assessed using a Bioanalyzer2100 with an RNA6000 NanoChip (Agilent Technologies, Amstelveen, The Netherlands) and an ND-1000 spectrophotometer (NanoDrop Technologies, DE, USA), respectively. The RNA integrity numbers of all samples were greater than 9.2. Briefly, duplicate samples consisting of 300 ng total RNA from NCI–H292 cells pretreated with Rg5 (0 or 50 μg/mL for 30 min) and treated with PMA (10 mg/mL for 1 h) were converted to double-stranded cDNA using random hexamers incorporating a T7 promoter. Amplified RNA was generated from the double-stranded cDNA template through an in vitro transcription reaction and purified with the Affymetrix sample cleanup module. cDNA was regenerated through random-primed reverse transcription using a dNTP mix containing dUTP. The cDNA was then fragmented by UDG and APE 1 restriction endonucleases and end-labeled using a terminal transferase reaction incorporating a biotinylated dideoxynucleotide. Fragmented end-labeled cDNA was hybridized to GeneChip Mouse Gene 2.0 ST arrays (Affymetrix, Santa Clara, CA, USA) for 17 h at 45°C and 60 rpm,

as described in the Gene Chip Whole Transcript Sense Target Labeling Assay Manual (Affymetrix). After hybridization, the chips were stained and washed in a Genechip Fluidics Station 450 (Affymetrix) and scanned using a Genechip Array scanner 3000 7G (Affymetrix). The raw data were deposited in the Gene Expression Omnibus (accession ID: GSE173990).

2.6. Identification of differentially expressed genes (DEGs)

The $\log_2$-probe-intensities obtained from the raw data using the 'oligo' package in R software (version 3.6) [17] were normalized using the quantile normalization method [18]. We then applied an integrative statistical method to the normalized $\log_2$-probe-intensities [19] to identify DEGs between NCI–H292 cells in the presence and absence of Rg5. Briefly, for each gene, we computed the observed *T*-value and $\log_2$-median-ratio between the two conditions using Student's *t*-test and $\log_2$-median-ratio test, respectively. Next, empirical null distributions of both *T*-values and $\log_2$-median-ratios were estimated by performing random permutation of the samples 1,000 times on the $\log_2$-probe-intensities. By applying two-tailed tests for the empirical distributions, we obtained the adjusted *P*-values for the observed *T*-value and $\log_2$-median-ratio of each gene, and the two adjusted *P*-values were combined into an overall *P*-value using Stouffer's method [20]. Finally, the DEGs were identified as genes with overall *P*-values < 0.1 and absolute $\log_2$-median-ratios > the cutoff, which was set as the mean of the 10th and 90th percentiles of the corresponding empirical distribution.

2.7. Enrichment analysis

We conducted functional enrichment analyses for the up- and downregulated DEGs in NCI–H292 cells treated with Rg5 using the DAVID software [21]. Gene Ontology biological processes (GOBPs) and Kyoto Encyclopedia of Genes and Genomes (KEGG) pathways with *P*-value < 0.05 and number of genes > 3 were identified as those significantly enriched by the DEGs.

2.8. Network analysis reconstruction of a molecular network model

To describe resolution-associated biological processes and signaling pathways mediated by Rg5 treatment, we reconstructed a molecular network model of the DEGs, which were annotated with lipid (cholesterol and glycerolipid) metabolism and the transforming growth factor (TGF)-β, mitogen-activated protein kinase (MAPK), and nuclear factor (NF)-κB signaling pathways. The interactions (edges) between the selected genes (nodes) in the network were identified based on 84,683 protein-protein interactions for 11,649 proteins obtained from the following 10 interactome databases: BioGRID, HuRI, IntAct, HitPredict, IID, MINT, STRING, HPRD, DIP, and the HTRIdb [22–30]. The network was visualized using Cytoscape software [31], and the nodes in the network were further arranged based on information from the KEGG pathway database.

2.9. BODIPY staining for flow cytometry

NCI–H292 cells were cultured in 60-mm cell culture dishes and incubated overnight at 37°C. Cells were then treated with 30 μM oleic acid (cat. O1008-5G; Sigma-Aldrich) as a control for more than 16 h. BODIPY493/503 staining solution (Thermofisher Scientific, Waltham, MA, USA) was dissolved in phosphate-buffered saline (PBS) at a concentration of 2 μM. The cells were incubated with BODIPY staining solution in the dark for 15 min at 37°C. Thereafter, the cells were washed with 3 mL PBS to remove media/serum and incubated with trypsin-ethylenediaminetetraacetic acid (0.25%) for 5 min at 37°C. Next, 5 mL PBS was added, and the cell suspension was transferred to a 15-mL conical tube and centrifuged at 16,600 × g for 15 min at 4°C. The supernatant was discarded, and the cell pellet was subjected to wash in 3 mL PBS, followed by centrifugation at 13,000 rpm for 15 min at 4°C. The supernatant was discarded, and the pellet resuspended in 300 μL flow cytometry buffer (0.1 M HEPES [pH 7.4], 1.4 M NaCl, 25 mM $CaCl_2$). Thereafter, the cell suspension was transferred to a fluorescence-assisted cell sorting tube, and flow cytometry was performed using a minimum of 10,000 events per condition.

2.10. BODIPY staining for microscopy

NCI–H292 cells were cultured on Lab-Tek chamber slides (Thermofisher Scientific) and incubated overnight with bovine serum albumin (BSA) or BSA-containing oleic acid. Cells were treated with Rg5 (0, 10, 25, or 50 μg/mL for 2 h), washed with 500 μL PBS, and incubated with BODIPY staining solution in the dark for 15 min at 37°C. The cells were washed with 1 mL PBS to remove the medium/serum. Thereafter, the cells were fixed with 4% paraformaldehyde in a PBS solution and washed with PBS three times for 5 min each. A drop of Prolong Gold antifade reagent with DAPI (Molecular Probes, Eugene, OR, USA) was added onto the slide as a mounting solution. Imaging was performed using an LSM800 confocal microscope (Zeiss, Jena, Germany) with the ZEN V3.4 software (Zeiss), and images were captured at 400× magnification. The relative intensity of BODIPY staining was measured using ImageJ software.

2.11. Reactive oxygen species (ROS) assay

Cellular ROS levels were measured using 20 μM 2'7'-dichlorofluorescin diacetate (DCFDA) dye (Molecular Probes, Eugene, OR, USA), a selective fluorescent indicator of ROS. NCI–H292 cells were seeded in 24-well plates at a density of 2×10^5 cells and incubated at 37°C for 24 h. Subsequently, the cells were pretreated either with NAC (1 mM for 30 min) or Rg5 (50 and 10 μg/mL for 30 min) and then treated with PMA (10 mg/mL for 30 min). For sampling, the cells were washed with HEPES controlled salt solution (HCSS; 120 mM NaCl, 5 mM KCl, 1.6 mM $MgCl_2$, 2.3 mM $CaCl_2$, 15 mM glucose, 20 mM HEPES, 10 mM NaOH, pH 7.4) and treated with 20 μM DCFDA dye for 30 min at 37°C. The cells were then washed with HCSS, and intracellular fluorescence was determined by measuring the fluorescence intensity at 485 and 530 nm (excitation and emission, respectively).

2.12. Western blot analysis

NCI–H292 cells were pretreated with Rg5 (0, 10, 50, or 100 μg/mL for 30 min), treated with PMA (10 mg/mL for 15 min), and then harvested using RIPA buffer as lysis buffer (Tris base, sodium chloride, Triton-X, sodium deoxycholate, EGTA). After centrifugation at 13,000 rpm for 15 min, the supernatant was removed, and the protein content of the lysate was quantified using BCA assays (cat. 23227; Thermofisher Scientific). Samples were boiled at 100°C for 10 min in sodium dodecyl sulfate polyacrylamide gel electrophoresis sample buffer, and 20 μg was loaded onto 15% polyacrylamide gels. Electrophoresis was performed at 100 V for 1–2 h. Proteins were transferred to polyvinylidene difluoride membranes (Roche, Basel, Switzerland) with a Trans-Blot Electrophoretic Transfer cell (Bio-Rad Laboratories, Hercules, CA, USA). Membranes were incubated for 1 h in blocking buffer (1% BSA in TBS) and then further incubated overnight at 4°C with the following primary antibodies: anti-extracellular signal-regulated kinase (ERK; cat.

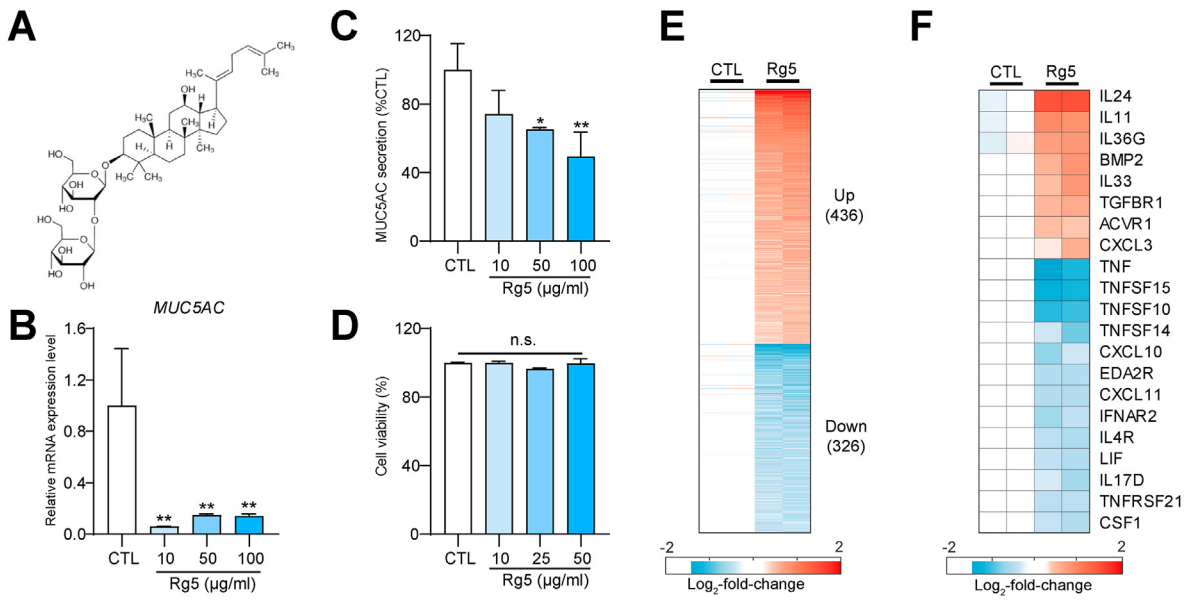

Fig. 1. Rg5 downregulated mucin overproduction and suppressed inflammation. (a) The chemical structure of the ginsenoside Rg5. (b) qPCR analysis of *MUC5AC* expression in NCI–H292 cells pretreated with Rg5 (0, 10, 50, or 100 μg/mL for 30 min) and treated with PMA (10 ng/mL for 1 h). Gene expression was normalized to *GAPDH* expression. (c) MUC5AC secretion analysis in NCI–H292 cells pretreated with Rg5 (0, 10, 50, or 100 μg/mL for 30 min) and treated with PMA (10 ng/mL for 30 min). (d) Cytotoxicity analysis in NCI–H292 cells treated with Rg5 (0, 10, 25, 50, or 100 μg/mL for 24 h), as assessed using MTT assays. (e) Heatmap showing expression patterns of DEGs in duplicate samples of NCI–H292 cells treated with Rg5 (0 or 50 μg/mL for 30 min) and PMA (10 mg/mL for 1 h). (f) Heatmap showing expression patterns of the anti- and pro-inflammatory genes, which were differentially expressed in duplicate samples of NCI–H292 cells treated with Rg5 (0 or 50 μg/mL for 30 min) and PMA (10 mg/mL for 1 h). *$P < 0.05$, **$P < 0.01$, as determined by one-way analysis of variance with a post hoc test (Dunnett's correction). DEG: differentially expressed gene; PMA: phorbol 12-myristate 13-acetate; MTT: 3-(4,5-dimethylthiazol-2-yl)-2,5-diphenyltetrazolium bromide; CTL: control.

4695), anti-phospho-ERK (cat. 9101), anti-p38 (cat. 9212), and anti-phospho-p38 (cat. 4631; all from Cell Signaling Technology, Beverly, MA, USA) diluted in TBS-T at 1:4000. The secondary antibody (GenDEPOT, Barker, TX, USA) was diluted at 1:5000 in TBS-T and incubated with the membranes for 1 h at room temperature. Bands were developed using SuperSignal West Pico PLUS Chemiluminescent Substrate (Thermofisher Scientific), and protein expression was detected using a Fusion Solo S chemiluminescence system (Koreabiomics, Seoul, Korea).

2.13. Statistical analysis

Statistical analyses of experimental results, including the results of ELISAs, DCFDA assays, flow cytometry, and cell viability assays, were performed using Prism v8 (GraphPad Software). Unpaired Student's *t*-tests and one-way analysis of variance with post-hoc tests (Dunnett's correction) were applied for comparisons between two groups and more than two groups, respectively, as indicated in the figure legends. Across all analyses, a *P*-value of less than 0.05 was considered statistically significant.

3. Results and discussion

3.1. Rg5 blocked MUC overproduction and alleviated inflammation

Ginsenosides have been studied as therapeutic agents for various diseases, and several recent studies have demonstrated that certain ginsenosides possess anti-inflammatory properties [32,33]. Because airway inflammatory diseases are associated with hypersecretion of MUCs, we first aimed to select a ginsenoside that could effectively decrease MUC production. Firstly, 16 saponins from *P. ginseng* (Fig. S1) were selected based on their distinct structures. Rg5, a ginsenoside originating from steamed ginseng (Fig. 1A), effectively reduced MUC5AC secretion (Fig. S1) and demonstrated similar significance as compound K (ComK), a ginsenoside involved in regulation of airway inflammation and mucus secretion**.** For that reason, Rg5 presented a potential inhibitory effect on the hyperactivation of mucosa cells and thus was selected as the target compound for this study [34]. Furthermore, Rg5 reduced *MUC5AC* mRNA levels (Fig. 1B) and suppressed MUC5AC secretion in a concentration-dependent manner (Fig. 1C). Importantly, all tested concentrations of Rg5 showed no cytotoxicity in the same cell line (Fig. 1D), indicating its possible applications as an anti-MUC production agent.

Next, to systematically investigate whether Rg5 contributed to the alleviation of inflammation, we performed microarray analysis and compared gene expression profiles in NCI–H292 cells in the absence and presence of Rg5. The comparative analysis identified 762 DEGs, consisting of 436 and 326 up- and downregulated genes in Rg5 treatment, respectively (Fig. 1E and Table S2). Among the 762 DEGs, there were 16 cytokine/receptor-encoding genes associated with pro-inflammatory responses and five genes associated with anti-inflammatory responses and the wound healing process (Fig. 1F and Table S3). Interestingly, among the 16 pro-inflammatory genes, downregulation was observed for 13, including tumor necrosis factor (*TNF*); TNF superfamily members 10, 14, and 15 (*TNFSF10*, *TNFSF14*, and *TNFSF15*); TNF receptor superfamily member 21 (*TNFRSF21*); ectodysplasin A2 receptor (*EDA2R*); C-X-C motif chemokine ligands 10 and 11 (*CXCL10* and *CXCL11*); interferon alpha and beta receptor subunit 2 (*IFNAR2*); interleukin 4 receptor (*IL4R*); LIF, interleukin 6 family cytokine (*LIF*); interleukin 17D (*IL17D*); and colony stimulating factor 1 (*CSF1*). By contrast, upregulation was observed for all five anti-inflammatory and wound healing-associated genes, i.e., interleukins 11 and 24 (*IL11* and *IL24*), bone morphogenetic protein 2 (*BMP2*), TGF-β receptor 1 (*TGFBR1*), and activin A receptor type 1 (*ACVR1*), suggesting the anti-inflammatory effects of Rg5.

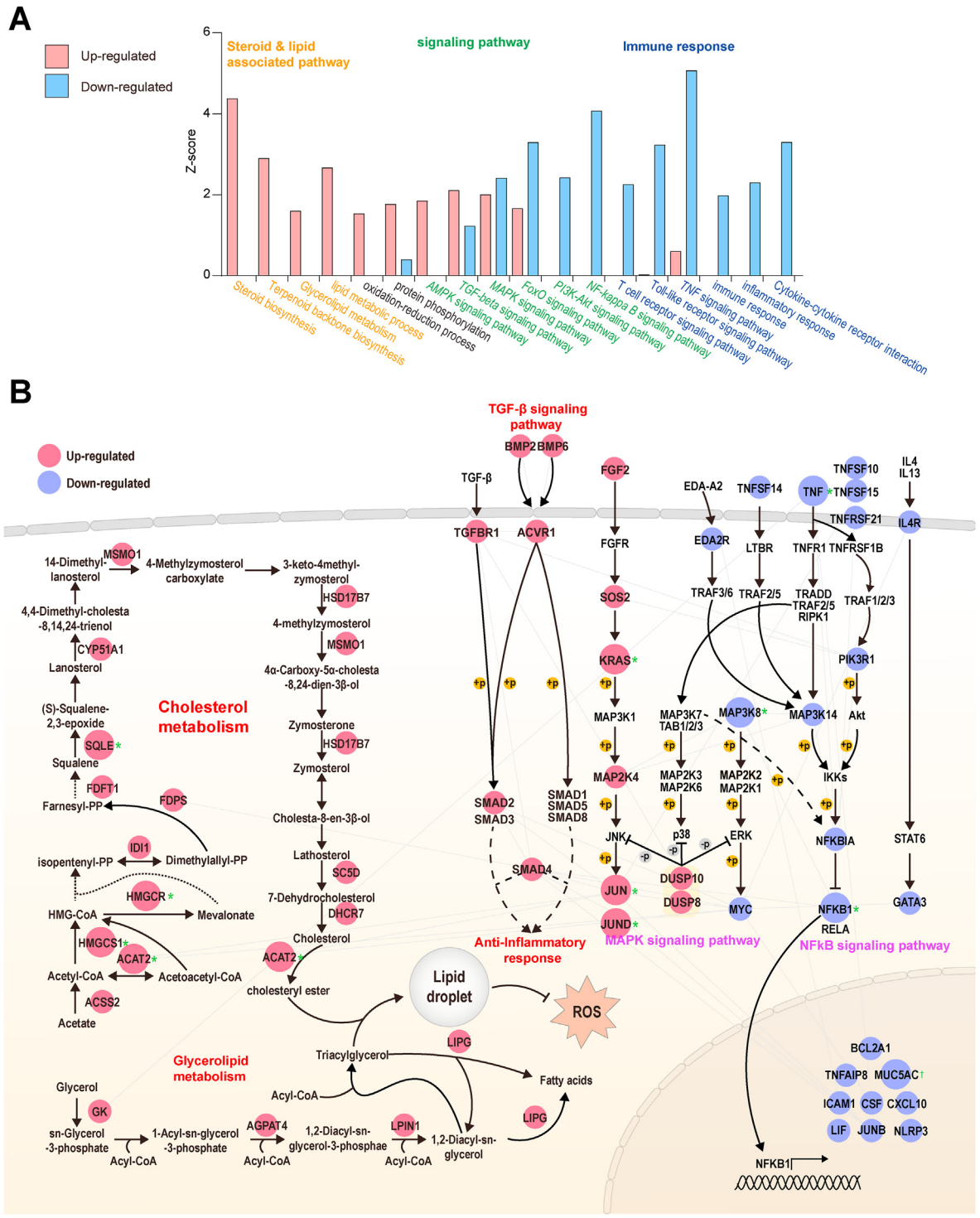

Fig. 2. Systematic exploration of resolution-associated signaling pathways, lipid droplet formation and subsequent ROS removal by Rg5. (a) GOBPs and KEGG pathways enriched by the genes depicted in Fig. 1E. Enrichment scores were converted to *Z*-scores, defined as $Z = N^{-1}(1 - P)$, where $N^{-1}(\cdot)$ is the inverse standard normal distribution and *P* is that enrichment *P* value. (b) Network model for the interactions among DEGs involved in several pathways. Pathways are based on the KEGG pathway database. The gray solid lines represent interactions among proteins; the *arrows* and *inhibition* symbol denote activation and suppression, respectively. The differential expression patterns of genes with large nodes were examined by qPCR. Small nodes with the symbol + p or −p denote phosphorylation and dephosphorylation, respectively. qPCR: quantitative real-time polymerase chain reaction; GOBP: Gene Ontology biological process; KEGG: Kyoto Encyclopedia of Genes and Genomes; DEGs: differentially expressed genes.

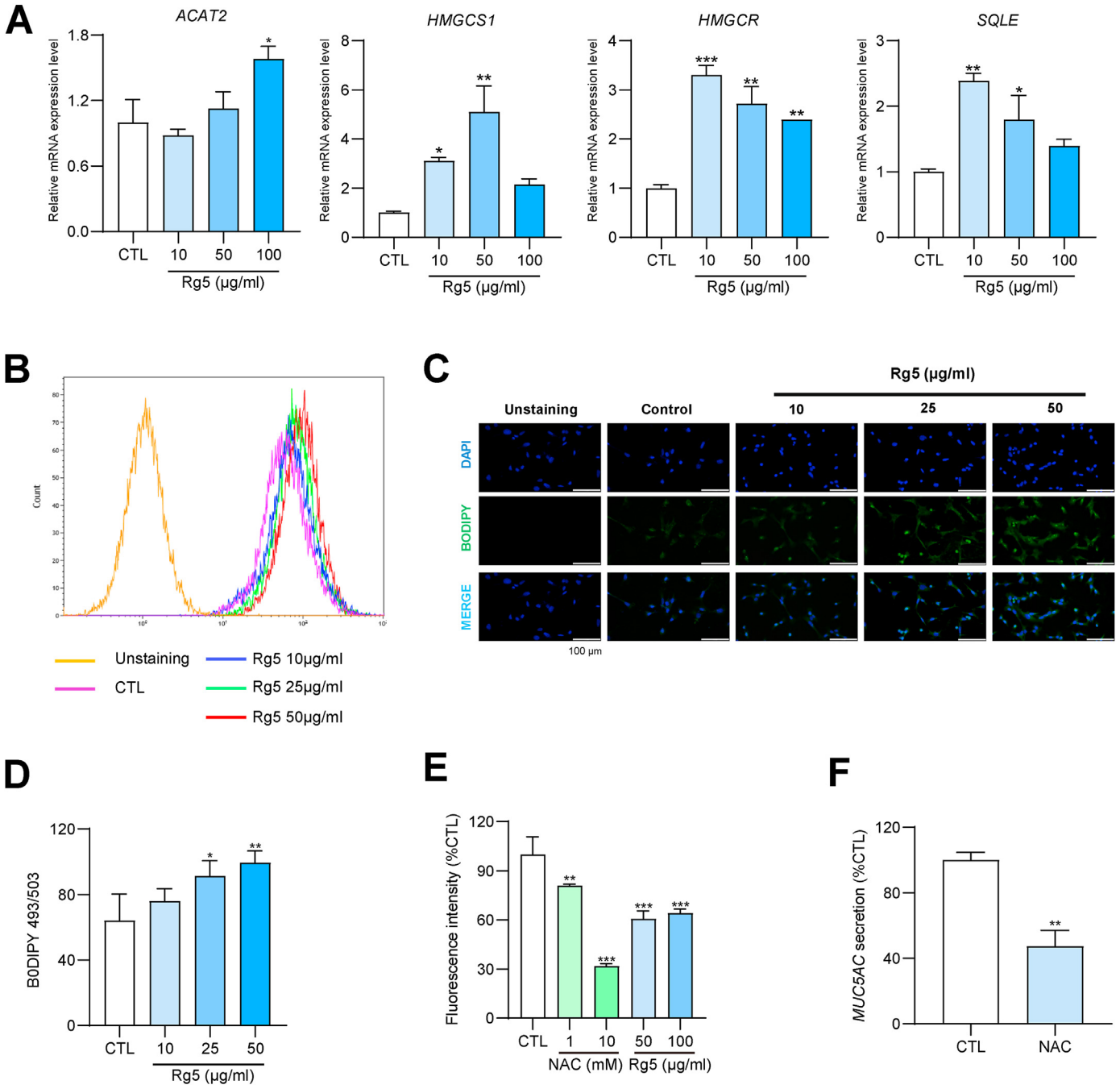

Fig. 3. Rg5 induced the accumulation of lipid droplets to consequently reduce ROS levels. (a) qPCR analysis of *ACAT2*, *HMGCS1*, *HMGCR*, and *SQLE* expression levels in NCI–H292 cells pretreated with Rg5 (0, 10, 50, or 100 μg/mL for 30 min) and treated with PMA (10 ng/mL for 1 h). (b) Flow cytometry analysis of NCI–H292 cells pretreated with Rg5 (0, 10, 25, or 50 μg/mL), treated with PMA (10 ng/mL for 30 min), and stained with BODIPY. (c) Confocal microscopy of NCI–H292 cells treated with Rg5 (0, 10, 25, or 50 μg/mL) and stained with the lipid droplet indicator BODIPY (green). Images were captured at a magnification of 400 × . Cell nuclei (blue) were stained with DAPI. (d) Relative intensity of BODIPY staining. (e) ROS assay of NCI–H292 cells were pretreated with NAC (1 or 10 mM for 30 min) or Rg5 (50 or 100 μg/mL for 30 min), treated with PMA (10 ng/mL for 30 min), and then incubated with DCFDA for 30 min. (f) MUC5AC secretion analysis in NCI–H292 cells pretreated with NAC (10 mM for 30 min) and treated with PMA (10 ng/mL for 30 min). $*P < 0.05$, $**P < 0.01$, $***P < 0.001$. qPCR: quantitative real-time polymerase chain reaction; PMA: phorbol 12-myristate 13-acetate; NAC: N-acetyl-L-cysteine; CTL: control.

3.2. Comprehensive transcriptome analysis of cellular processes and signaling pathways involved in Rg5-mediated inflammatory resolution

To systematically investigate the cellular processes and signaling pathways that may contribute to the anti-inflammatory response, we performed functional enrichment analysis of GOBPs and KEGG pathways for the up- and downregulated genes (Fig. 2A and Table S4). The upregulated genes significantly ($P < 0.05$) represented i) lipid metabolism (steroid and terpenoid backbone biosynthesis and glycerolipid metabolism) and oxidation-reduction processes and ii) protein phosphorylation and signaling pathways (AMP-activated protein kinase, TGF-β, MAPK, and FoxO signaling), whereas the downregulated genes represented i) signaling pathways (MAPK, FoxO, phosphatidylinositol 3-kinase/AKT, and NF-κB signaling) and ii) inflammatory and immune responses (T cell

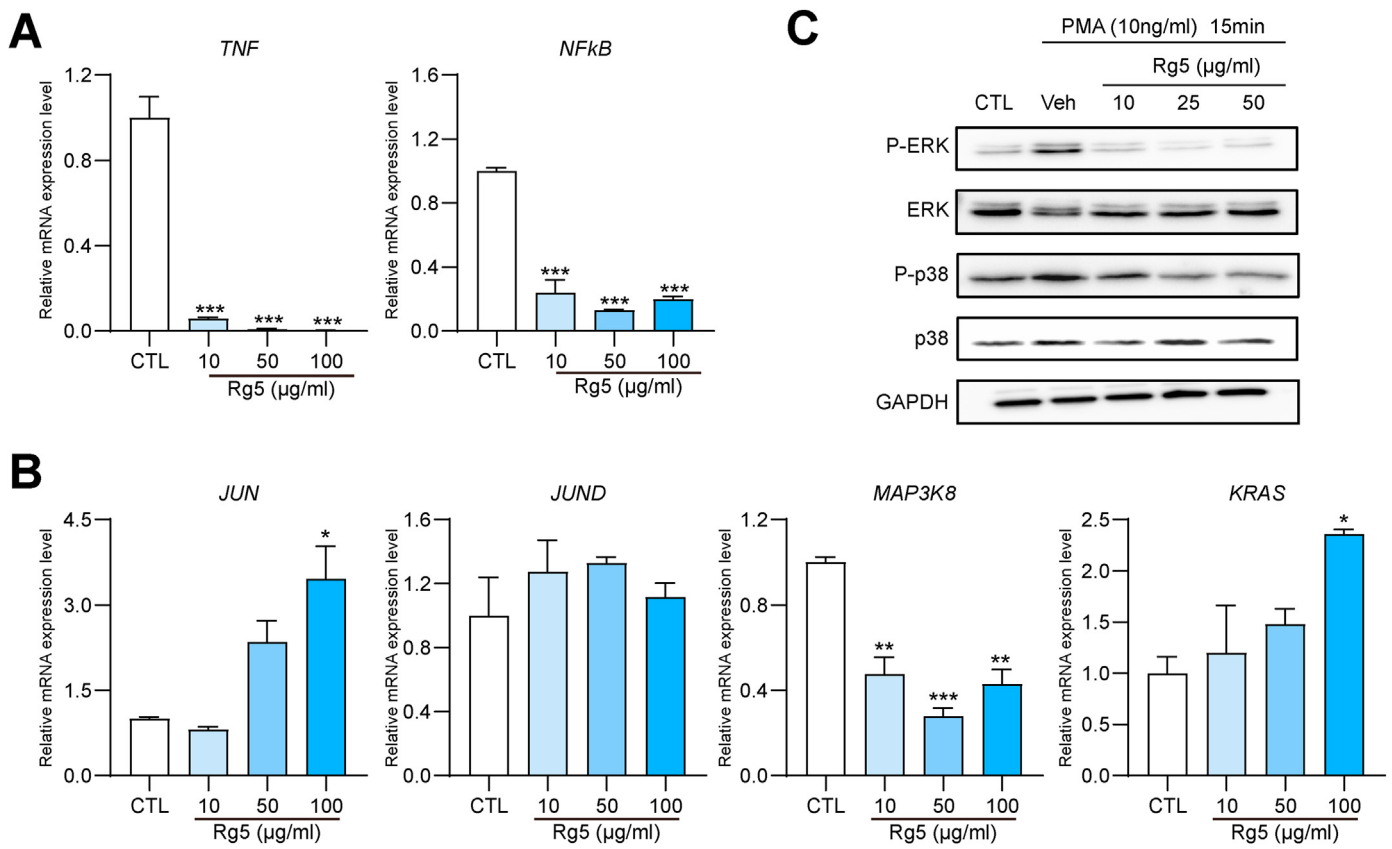

Fig. 4. Rg5 inhibited the MAPK signaling pathway and the production of pro-inflammatory cytokines. (a) qPCR analysis of pro-inflammatory genes (*TNF*, *NF-κB*) in NCI–H292 cells pretreated with Rg5 (0, 10, 50, or 100 μg/mL for 30 min) and treated with PMA (10 ng/mL for 1 h). (b) qPCR analysis of MAPK-associated genes (*JUN*, *JUND*, *MAP3K8*, and *KRAS*) in NCI–H292 cells pretreated with Rg5 (0, 10, 50, or 100 μg/mL for 30 min) and treated with PMA (10 ng/mL for 1 h). (c) Western blot analysis of ERK, p38, phosphorylated ERK, and phosphorylated p38 protein levels in NCI–H292 cells pretreated with Rg5 (0, 10, 25, or 50 μg/mL for 30 min) and treated with PMA (10 ng/mL for 15 min). GAPDH was used as a loading control. $*P < 0.05$, $**P < 0.01$, $***P < 0.001$. qPCR: quantitative real-time polymerase chain reaction; PMA: phorbol 12-myristate 13-acetate; CTL: control.

receptor, Toll-like receptor, and TNF signaling pathways and cytokine-cytokine receptor interaction).

We then generated a network model that described the interactions among the DEGs and MUC5AC to provide insights into the enriched cellular processes and signaling pathways at the molecular level (Fig. 2B). The upregulated genes in Rg5-treated cells were involved in cholesterol (*ACSS2*, *ACAT2*, *HMGCS1*, *HMGCR*, *IDI1*, *FDPS*, *FDFT1*, *SQLE*, *CYP51A1*, *MSMO1*, *HSD17B7*, *SC5D*, and *DHCR7*) and glycerolipid metabolism (*GK*, *AGPAT4*, *LPIN1*, and *LIPG*), which may induce the accumulation of lipid droplets to facilitate ROS clearance, and were also involved in the TGF-β signaling pathway (*BMP2*, *BMP6*, *TGFBR1*, *ACVR1*, *SMAD2*, and *SMAD4*), which may activate anti-inflammatory responses. By contrast, the downregulated genes were involved in TNF and NF-κB signaling pathways (*TNF*, *TNFSF10*, *TNFSF14*, *TNFSF15*, *TNFSF21*, *IL4R*, *EDA2R*, *PIK3R1*, *MAP3K14*, *NFKBIA*, *NFKB1*, and *GATA3*) and their downstream targets (*BCL2A1*, *TNFAIP8*, *MUC5AC*, *ICAM1*, *CSF*, *CXCL10*, *LIF*, *JUNB*, and *NLRP3*), thereby suppressing pro-inflammatory responses. Intriguingly, c-Jun N-terminal kinase and ERK signaling pathways, which are both MAPK signaling pathways, were regulated in opposite directions by the upregulated genes (*FGF2*, *SOS2*, *KRAS*, *MAPK2K4*, *DUSP8*, *DUSP10*, *JUN*, and *JUND*) and downregulated genes (*MAP3K8* and *MYC*), respectively. Collectively, these findings provided insights into the molecular mechanisms through which Rg5 may exert its beneficial effects.

3.3. Rg5 induced the accumulation of lipid droplets to reduce ROS levels

Rg5 has been linked to the regulation of several metabolic pathways, including regulation of lipid and glucose homeostasis [35]. In addition, unlike other ginsenosides, Rg5 is easily digested by lysosomes, further indicating its advantages in cellular lipid synthesis [36]. Based on our network model presented in Fig. 2B, we examined whether cellular ROS levels were reduced via the functions of the lipid droplets formed following Rg5 treatment. To this end, we selected key genes involved in cholesterol metabolism, such as acetyl-CoA acetyltransferase 2 (*ACAT2*), 3-hydroxy-3-methylglutaryl-CoA synthase 1 (*HMGCS1*), 3-hydroxy-3-methylglutaryl-CoA reductase (*HMGCR*), and squalene epoxidase (*SQLE*), and evaluated the expression of these genes using qPCR (Fig. 3A). These genes were readily upregulated by Rg5 treatment, as shown in our network model based on microarray data (Fig. 2B). Next, the abundances of lipid droplets were measured in control cells and cells treated with different concentrations of Rg5 via flow cytometry and fluorescence microscopy using the BODIPY-conjugated lipid droplet indicator (Fig. 3B, C, and D). The results showed that Rg5 intensified BODIPY signals, indicating an increase in lipid droplets. Consistent with this, cellular ROS levels were also reduced after Rg5 treatment (Fig. 3E). Furthermore, NAC, a ROS inhibitor, readily reduced MUC5AC secretion (Fig. 3F), suggesting that clearance of ROS by Rg5-induced lipid droplets contributed to the reduction of MUC levels in mucosa cells.

3.4. Rg5 regulated the activation of MAPK and NF-κB signaling pathways for anti-inflammatory responses in mucosal cells

Our network model suggested that MAPK and NF-κB signaling pathways, which are involved in the resolution of inflammation as well as modulation of *MUC5AC* expression [37,38], were regulated by Rg5 treatment (Fig. 2B). To further test this hypothesis, the differential regulation of MAPK and NF-κB signaling pathways by Rg5 treatment was confirmed by qPCR analysis (Fig. 4A and B). For the NF-κB signaling pathway, the mRNA levels of *TNF* and *NF-κB* were significantly ($P < 0.001$) decreased after Rg5 treatment (Fig. 4A). For the MAPK signaling pathway, we confirmed the significant ($P < 0.05$) upregulation of *JUN* and *KRAS* and the significant downregulation of *MAP3K8* (Fig. 4B), consistent with our network model. Furthermore, MUC5AC secretion was found to be dependent on the phosphorylation of ERK and p38, key kinases in the MAPK signaling pathway, which are involved in the activation of NF-κB and the production of pro-inflammatory cytokines; indeed, treatment with inhibitory compounds decreased MUC5AC secretion (Fig. S2). Hence, in addition to transcriptional regulation, our western blot analysis revealed that phosphorylation of ERK and p38 proteins was repressed by Rg5 treatment (Fig. 4C). Collectively, these results supported the regulatory effects of Rg5 on inflammation-associated signaling pathways, as suggested by our network model (Fig. 2B).

4. Conclusions

In the current study, a combination of systematic transcriptome analysis and molecular biology experiments revealed that Rg5 upregulated lipid metabolism, thereby contributing to the lipid droplet-mediated clearance of ROS, and modulated the activation of the MAPK and NF-κB signaling pathways. As described in hyperactivated airway mucosa cells show increased inflammatory responses, resulting in the expression of pro-inflammatory cytokines. Simultaneously, extracellular matrix synthesis and MUC expression are augmented, leading to blockage of the airway. After Rg5 treatment, the mucosa cells showed reduction of hyperactivation, and this effect may help to alleviate respiratory disorders. These findings provided valuable insights into the development of new approaches to alleviate respiratory disorders. Further studies of Rg5 treatment in combination with animal model experiments and clinical analyses are warranted.

During normal lipid metabolism, epithelial cells are capable of modulating homeostasis and inhibiting mechanisms associated with inflammation through a variety of regulatory mechanisms, including growth factors, cytokines, and chemokine [38–40]. In the context of respiratory diseases, epithelial cells lose their ability to regulate lipid metabolism, and oxidative stress releases inflammatory mediators, leading to lung diseases, such as loss of pulmonary function, airway hypersensitivity, mucus hypersecretion, and lung remodeling; this in turn results in abnormal recovery mechanisms [41,42]. For example, TNF and NF-κB, which regulate the expression of several genes involved in the immune response (Fig. 2B), have been shown to be overexpressed in patients with asthma, which is a serious refractory disease [43,44]. In addition, p38 MAPK activation is initiated via a kinase cascade triggered by extracellular inflammatory stimulation and induces apoptosis in human airway epithelial cells [45]. Therefore, inflammatory drugs capable of targeting molecules involved in lung pathways may prove to be useful in the treatment of respiratory diseases [4,46]. Additionally, targeting lipid metabolism pathways and molecules could contribute to superior treatment approaches by regulating lipid homeostasis and mucus production [47].

Furthermore, compared with other ginsenosides, Rg5 showed better inhibitory effects on MUC production. Low-polarity ginsenosides, such as Rg5, are associated with better anti-inflammatory activity in comparison to polar ginsenosides [48–50]. In addition, Rg5 not only has anti-allergic effects but also exhibits better pharmacokinetic properties compared with other ginsenosides [51–53]. Therefore, we propose that the structural conformation of Rg5 may facilitate better cellular uptake, leading to improved metabolic responses. In the future, a more extensive and functional system as well as diverse screening and evaluation methods are necessary to further elucidate the potential applications of ginsenosides in human health.

Acknowledgements

We would like to thank Editage for the English language editing. The current study was supported by grants from the National Research Foundation of Korea (NRF) funded by the Korean government (MSIT) (grant no. 2019005607 to B.H.B. and grant no. 2020M3A9I6A01036057 to J.H.P.), the Rural Development Administration(grant no. PJ014868042022 by M.G.L.), the Korea Research Institute of Bioscience and Biotechnology (KRIBB) Research Initiative Program (grant no. KGM5422221 to J.H.P.), the Ajou University Research Fund (B.H.B.), and the Gyeonggido Business & Science Accelerator (GBSA) grant.

Appendix A. Supplementary data

Supplementary data to this article can be found online at https://doi.org/10.1016/j.jgr.2022.06.001.

References

[1] Barnes PJ. The role of inflammation and anti-inflammatory medication in asthma. Respir Med 2002;96(Suppl):S9–15.
[2] Kesimer M, et al. Airway mucin concentration as a marker of chronic bronchitis. New England Journal of Medicine 2017;377(10):911–22.
[3] Bonser LR, Erle DJ. Airway mucus and asthma: the role of MUC5AC and MUC5B. J Clin Med 2017;6(12).
[4] Rogers DF. Physiology of airway mucus secretion and pathophysiology of hypersecretion. Respir Care 2007;52(9):1134–46. discussion 1146-9.
[5] Li J, Ye Z. The potential role and regulatory mechanisms of MUC5AC in chronic obstructive pulmonary disease. Molecules 2020;25(19):4437.
[6] Kim V, et al. Persistent and newly developed chronic bronchitis are associated with worse outcomes in chronic obstructive pulmonary disease. Ann Am Thorac Soc 2016;13(7):1016–25.
[7] Jin F, et al. Diclofenac inhibits phorbol ester-induced gene expression and production of MUC5AC mucin via affecting degradation of IkBα and translocation of NF-kB p65 in NCI-H292 cells. Biomol Ther (Seoul) 2020;28(5):431–6.
[8] Pan SY, et al. New perspectives on how to discover drugs from herbal medicines: CAM's outstanding contribution to modern therapeutics, vol. 2013. Evid Based Complement Alternat Med; 2013, 627375.
[9] Süntar I. Importance of ethnopharmacological studies in drug discovery: role of medicinal plants. Phytochemistry Reviews 2020;19(5):1199–209.
[10] Hwang CR, et al. Changes in ginsenoside compositions and antioxidant activities of hydroponic-cultured ginseng roots and leaves with heating temperature. J Ginseng Res 2014;38(3):180–6.
[11] Qi HY, Li L, Ma H. Cellular stress response mechanisms as therapeutic targets of ginsenosides. Med Res Rev 2018;38(2):625–54.
[12] Leung KW, Wong AS. Pharmacology of ginsenosides: a literature review. Chin Med 2010;5:20.
[13] Kim TW, et al. Ginsenoside Rg5 ameliorates lung inflammation in mice by inhibiting the binding of LPS to toll-like receptor-4 on macrophages. Int Immunopharmacol 2012;12(1):110–6.
[14] Feng SL, et al. Ginsenoside Rg5 overcomes chemotherapeutic multidrug resistance mediated by ABCB1 transporter: in vitro and in vivo study. J Ginseng Res 2020;44(2):247–57.
[15] Li W, et al. Ginsenoside Rg5 ameliorates cisplatin-induced nephrotoxicity in mice through inhibition of inflammation, oxidative stress, and apoptosis. Nutrients 2016;8(9).
[16] Lee YY, et al. Anti-inflammatory effect of ginsenoside Rg5 in lipopolysaccharide-stimulated BV2 microglial cells. Int J Mol Sci 2013;14(5):9820–33.

[17] Carvalho BS, Irizarry RA. A framework for oligonucleotide microarray preprocessing. Bioinformatics 2010;26(19):2363–7.
[18] Bolstad BM, et al. A comparison of normalization methods for high density oligonucleotide array data based on variance and bias. Bioinformatics 2003;19(2):185–93.
[19] Lee HJ, et al. Direct transfer of alpha-synuclein from neuron to astroglia causes inflammatory responses in synucleinopathies. J Biol Chem 2010;285(12):9262–72.
[20] Hwang D, et al. A data integration methodology for systems biology. Proc Natl Acad Sci U S A 2005;102(48):17296–301.
[21] Huang da W, Sherman BT, Lempicki RA. Systematic and integrative analysis of large gene lists using DAVID bioinformatics resources. Nat Protoc 2009;4(1):44–57.
[22] Stark C, et al. BioGRID: a general repository for interaction datasets. Nucleic Acids Res 2006;34(issue):D535–9.
[23] Luck K, et al. A reference map of the human binary protein interactome. Nature 2020;580(7803):402–8.
[24] Orchard S, et al. The MIntAct project–IntAct as a common curation platform for 11 molecular interaction databases. Nucleic Acids Res 2014;42(issue):D358–63.
[25] López Y, Nakai K, Patil A. HitPredict version 4: comprehensive reliability scoring of physical protein-protein interactions from more than 100 species. Oxford): Database; 2015. 2015.
[26] Kotlyar M, et al. IID 2018 update: context-specific physical protein-protein interactions in human, model organisms and domesticated species. Nucleic Acids Res 2019;47(D1):D581–9.
[27] Szklarczyk D, et al. STRING v11: protein-protein association networks with increased coverage, supporting functional discovery in genome-wide experimental datasets. Nucleic Acids Res 2019;47(D1):D607–13.
[28] Goel R, et al. Human protein reference database and human proteinpedia as discovery resources for molecular biotechnology. Mol Biotechnol 2011;48(1):87–95.
[29] Salwinski L, et al. The database of interacting proteins: 2004 update. Nucleic Acids Res 2004;32:D449–51. Database issue).
[30] Bovolenta LA, Acencio ML, Lemke N. HTRIdb: an open-access database for experimentally verified human transcriptional regulation interactions. BMC Genomics 2012;13:405.
[31] Shannon P, et al. Cytoscape: a software environment for integrated models of biomolecular interaction networks. Genome Res 2003;13(11):2498–504.
[32] Attele AS, Wu JA, Yuan CS. Ginseng pharmacology: multiple constituents and multiple actions. Biochem Pharmacol 1999;58(11):1685–93.
[33] Piao X, et al. *Advances In Saponin Diversity Of Panax Ginseng.* Molecules 2020;25(15).
[34] Lee JW, et al. Compound K ameliorates airway inflammation and mucus secretion through the regulation of PKC signaling in vitro and in vivo. J Ginseng Res 2022;46(3):496–504.
[35] Xiao N, et al. Ginsenoside Rg5 inhibits succinate-associated lipolysis in adipose tissue and prevents muscle insulin resistance. Frontiers in Pharmacology 2017;8.
[36] Song L, et al. Ginsenoside Rg5 inhibits cancer cell migration by inhibiting the nuclear factor-κB and erythropoietin-producing hepatocellular receptor A2 signaling pathways. Oncol Lett 2021;21(6):452.
[37] Desmet C, et al. Selective blockade of NF-κB activity in airway immune cells inhibits the effector phase of experimental asthma. The Journal of Immunology 2004;173(9):5766–75.
[38] Calvén J, Ax E, Rådinger M. The airway epithelium-A central player in asthma pathogenesis. Int J Mol Sci 2020;21(23).
[39] Xiao C, et al. Defective epithelial barrier function in asthma. J Allergy Clin Immunol 2011;128(3):549–56. e1-556.
[40] Amatngalim GD, Hiemstra PS. Airway epithelial cell function and respiratory host defense in chronic obstructive pulmonary disease. Chin Med J (Engl) 2018;131(9):1099–107.
[41] Morgan BW, et al. Epidemiology and risk factors of asthma-chronic obstructive pulmonary disease overlap in low- and middle-income countries. J Allergy Clin Immunol 2019;143(4):1598–606.
[42] Zinellu E, et al. Circulating biomarkers of oxidative stress in chronic obstructive pulmonary disease: a systematic review. Respir Res 2016;17(1):150.
[43] Pelaia C, et al. Role of p38 mitogen-activated protein kinase in asthma and COPD: pathogenic aspects and potential targeted therapies. Drug Des Devel Ther 2021;15:1275–84.
[44] Brightling C, Berry M, Amrani Y. Targeting TNF-alpha: a novel therapeutic approach for asthma. J Allergy Clin Immunol 2008;121(1):5–10. ; quiz 11-2.
[45] Richards CD, et al. Regulation of IL-33 by oncostatin M in Mouse lung epithelial cells, vol. 2016. Mediators Inflamm; 2016, 9858374.
[46] Banerjee A, Koziol-White C, Panettieri Jr R. p38 MAPK inhibitors, IKK2 inhibitors, and TNFα inhibitors in COPD. Curr Opin Pharmacol 2012;12(3):287–92.
[47] Chen H, et al. Lipid metabolism in chronic obstructive pulmonary disease. Int J Chron Obstruct Pulmon Dis 2019;14:1009–18.
[48] Zhang F, et al. Stem-leaves of Panax as a rich and sustainable source of less-polar ginsenosides: comparison of ginsenosides from Panax ginseng, American ginseng and Panax notoginseng prepared by heating and acid treatment. J Ginseng Res 2021;45(1):163–75.
[49] Kwon SW, et al. Liquid chromatographic determination of less polar ginsenosides in processed ginseng. J Chromatogr A 2001;921(2):335–9.
[50] Feng J, et al. Comparison of the anti-inflammatory effects of different polar ginsenosides on rheumatoid arthritis. Industrial Crops and Products 2022;181:114845.
[51] Nag SA, et al. Ginsenosides as anticancer agents: in vitro and in vivo activities, structure-activity relationships, and molecular mechanisms of action. Front Pharmacol 2012;3:25.
[52] Shin Y-W, , B.E.-A., Han M-J, Kim D-H. Metabolism of ginsenoside Rg5, a main constituent isolated from RedGinseng, by human intestinal microflora and their antiallergic effect. Journal of Microbiology and Biotechnology 2006;16(11):1791–8.
[53] Ma C, et al. Pharmacokinetic studies of ginsenosides Rk1 and Rg5 in rats by UFLC–MS/MS. Biomedical Chromatography 2021;35(8):e5108.